Covalent Nitrogen Doping in Molecular Beam Epitaxy-Grown and Bulk WSe_2

UT Dallas Author(s):

Rafik Addou
Christopher M. Smyth
Ruoyu Yue
Christopher R. Cormier
Jiyoung Kim
Christopher L. Hinkle
Robert M. Wallace

Citation:

Khosravi, A., R. Addou, C. M. Smyth, R. Yue, et al. 2018. "Covalent nitrogen doping in molecular beam epitaxy-grown and bulk WSe_2." APL Materials 6(2), doi:10.1063/1.5002132

Covalent nitrogen doping in molecular beam epitaxy-grown and bulk WSe_2

Ava Khosravi, Rafik Addou, Christopher M. Smyth, Ruoyu Yue, Christopher R. Cormier, Jiyoung Kim, Christopher L. Hinkle, and Robert M. Wallace[a]

Department of Materials Science and Engineering, The University of Texas at Dallas, 800 West Campbell Road, Richardson, Texas 75080, USA

(Received 29 August 2017; accepted 8 November 2017; published online 8 January 2018)

Covalent *p*-type doping of WSe_2 thin films grown by molecular beam epitaxy and WSe_2 exfoliated from bulk crystals is achieved via remote nitrogen plasma exposure. X-ray photoelectron and Raman spectroscopies indicate covalently bonded nitrogen in the WSe_2 lattice as well as tunable nitrogen concentration with N_2 plasma exposure time. Furthermore, nitrogen incorporation induces compressive strain on the WSe_2 lattice after N_2 plasma exposure. Finally, atomic force microscopy and scanning tunneling microscopy reveal that N_2 plasma treatment needs to be carefully tuned to avoid any unwanted strain or surface damage. https://doi.org/10.1063/1.5002132

Transition metal dichalcogenides (TMDs), a family of two-dimensional (2D) materials with layered structure, have gained much attention recently due to their unique material properties like atomic-scale thickness, sizeable bandgap, and potential applications in various electronic and optoelectronic devices such as tunneling field-effect transistors (FETs), p-n diodes, and photovoltaics.[1–4] Tungsten diselenide (WSe_2) is among the most promising candidates for implementation of a TMD-based channel in next generation FETs due to its indirect-to-direct bandgap transition from bulk (~1.2 eV) to monolayer (~1.8 eV) and high *p*-type mobility up to 500 cm^2/V-s at room temperature.[5–7] Controllable and reliable doping of TMDs is essential for realizing commercially viable TMD-based devices. Various techniques have been employed in efforts to dope WSe_2 such as a "mild" He or H_2 plasma treatment to create anion Se vacancies,[8] Octadecyltrichlorosilane (OTS) and hexane solution treatment,[9] SiN_x deposition on WSe_2,[10] potassium doping of WSe_2 using a K dispenser,[11] and Au decoration of WSe_2 using thermal evaporation,[12] none of which involve substitutional doping. Other methods such as adsorption of NO_2 molecules on WSe_2 lead to substitutional doping;[13] however, the formation of various $WSe_{2-x-y}O_xN_y$ species with different oxidation states was detected. A more manufacturable approach, using a remote N_2 plasma, has also been employed previously to introduce nitrogen into the graphene lattice (among other materials).[14,15] Recently, this remote N_2 plasma method was reported as a successful method for controllable doping of exfoliated MoS_2.[16] In this work, we extend and compare the effect of similar N_2 plasma treatment on bulk WSe_2 and also on a few monolayers of WSe_2 grown by molecular beam epitaxy (MBE).

WSe_2 samples (thickness $\leq$ 7 layers) were grown via MBE on highly ordered pyrolytic graphite (HOPG) substrates provided by Momentive Performance Materials. The HOPG substrates were freshly exfoliated prior to being loaded into vacuum, followed by annealing at the 550 °C growth temperature for 1 h. Once the HOPG surface preparation was finished, the 2 h MBE growth of WSe_2 commenced with a W flux pressure of 7×10^{-9} mbar and a Se flux pressure of 1×10^{-6} mbar. Samples were slowly cooled down under a Se environment, and RHEED was performed *in situ* resulting in streaky patterns indicative of high-quality, smooth films.[17] The MBE samples were then removed from the growth chamber for the *ex situ* nitrogen doping experiments.

[a]Author to whom correspondence should be addressed: rmwallace@utdallas.edu

Bulk WSe_2 crystals, grown by chemical vapor transport (CVT) and purchased from HQ Graphene, were exfoliated in air using Scotch® Magic™ tape. Immediately following bulk WSe_2 exfoliation, both non-exfoliated MBE and exfoliated bulk WSe_2 samples were mounted on the same Mo-plate and loaded into an ultra-high vacuum (UHV) system described elsewhere[18] in less than 10 min. Samples were heated to 300 °C under UHV and held at this temperature for 2 h (base pressure $\sim 10^{-9}$ mbar) to remove physisorbed species induced by air exposure following exfoliation. Subsequently, the samples were exposed to a N_2 plasma, remotely generated via 13.56 MHz Radio Frequency (RF) at a power of 100 W under 45 SCCM nitrogen gas flow, for different sets of exposure time with an operation pressure of $\sim 7 \times 10^{-3}$ mbar. To study the surface chemistry after each treatment, the samples were transferred through a UHV transfer tube to an analysis chamber with a base pressure of $\sim 10^{-10}$ mbar equipped with X-ray photoelectron spectroscopy (XPS) described elsewhere.[18] The software *AAnalyzer* was used for XPS peak analysis. Active Shirley background and Voigt line shape was employed for peak fitting.[19] Raman and photoluminescence (PL) spectroscopy were employed to investigate the characteristic vibrational modes and optical bandgap of monolayer and bilayer WSe_2 flakes and films before and after 10 min N_2 plasma treatment. For Raman and PL measurements, few layers WSe_2 samples were prepared by mechanically exfoliating the bulk WSe_2 crystal and transferring them to thermally grown 270 nm SiO_2/Si substrates. Raman and PL spectra were acquired via 532 nm wavelength laser with a spot size of ~500 nm and 0.22 mW power under ambient conditions. An atomic force microscope (AFM), Veeco, Model 3100 Dimension V, operating in the tapping mode under ambient conditions was also used to characterize the surface morphology *ex situ* before and after the N_2 plasma treatment. In a separate UHV system equipped with an *Omicron* variable temperature scanning tunneling microscope (VT-STM),[20] room temperature STM and scanning tunneling spectroscopy (STS) were employed to compare the surface morphology and electronic structure of the MBE WSe_2 films before and after the N_2 plasma treatment. AFM and STM images were processed with the *WSxM* software.[21]

Figures 1(a)–1(c) show the W 4*f*, Se 3*d*, W $5p_{3/2}$, and N 1*s* core level spectra obtained from as-grown MBE WSe_2 and as-exfoliated WSe_2. Only spectral features associated with WSe_2 in the W 4*f* and Se 3*d* core level spectra are detected, which indicates initial WSe_2 surface oxidation is below detectable limits despite 10 min air exposure prior to loading into the UHV cluster tool. A small amount of adventitious carbon and oxygen are detected on the surface due to the short air exposure prior to loading into UHV as evidenced by the low-intensity chemical states detected

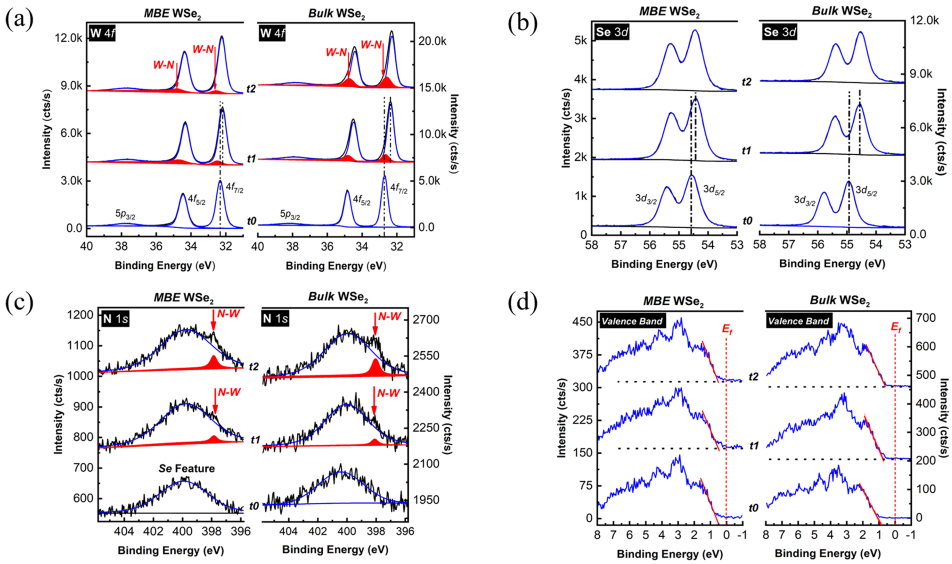

FIG. 1. [(a)–(d)] W *4f*, Se *3d*, W $5p_{3/2}$, and N 1*s* core level spectra and valence band spectra obtained from MBE and bulk, exfoliated WSe_2. t0 spectra are associated with as-grown MBE WSe_2 and as-exfoliated WSe_2, t1 with WSe_2 after 10 min N_2 exposure, and t2 with WSe_2 after 15 min N_2 exposure.

in C 1*s* and O 1*s* in Fig. S1 of the supplementary material. In order to remove these undesired species and also prevent the formation of CN_x during N_2 plasma treatment, samples were annealed at 300 °C for 2 h under UHV conditions.[16] It is important to note that prior to the N_2 plasma treatment, the N 1*s* core level region is convoluted with a broad Se feature at 400.0 eV, as shown in Fig. 1(c). Nitrogen remains below the XPS detection limit following N_2 plasma treatment for less than 10 min. For exposure times ≥10 min, the binding energy of the chemical state detected in the N 1*s* core level (397.9 eV) is consistent with previous reports of a transition metal-nitrogen bond.[22,23] An additional chemical state is detected in the W 4*f* core level obtained from both MBE and bulk WSe_2 at ~0.3 eV higher binding energy to that of W–Se after 10 min N_2 plasma exposure. The binding energy of the chemical state detected in the N 1*s* core level, in conjunction with the additional chemical state detected in the W 4*f* core level after 10 min N_2 plasma exposure, suggests the formation of covalent W–N bonds during the N_2 plasma treatment. Previous reports on W–N chemical states have shown similar binding energies to those reported here.[22–24] The detection of chemical states consistent with covalent W–N bonding in the W 4*f* and N 1*s* core level spectra obtained from both MBE and bulk WSe_2 samples suggests nitrogen incorporation into WSe_2 through Se substitution.

No additional chemical state was detected in the Se 3*d* core level aside from that of WSe_2 through all N_2 plasma exposure times investigated in this work, which indicates Se–N bond formation, if any, is below the limit of detection by XPS. After 20, 30, and 60 min exposure time, the intensity of the chemical state detected in the N 1*s* core level obtained from both MBE and bulk WSe_2 gradually increases (Fig. S2 of the supplementary material). Increasing the N_2 plasma exposure time results in an increased nitrogen to tungsten ratio and corresponding decrease in the selenium to tungsten ratio in WN_xSe_{2-x}. After 60 min N_2 plasma exposure, x = 0.17 for MBE WSe_2 and x = 0.16 for bulk WSe_2 as calculated from the XPS data. It should be noted that the W–N bond represents the only nitrogen species detected in either sample after N_2 plasma exposure of any duration. According to angle resolved XPS (ARXPS) performed at a bulk sensitive angle (75°) *versus* a surface sensitive angle (45°), the remote N_2 plasma exposure introduces nitrogen to the surface of WSe_2 samples (Fig. S3 of the supplementary material). Taken together, the ARXPS and detected surface chemical states are consistent with Se replacement by N from the remote plasma process, analogous to that reported for MoS_2.

The XPS spectra also shows a clear shift to lower binding energy by the same amount for all core levels, indicative of a Fermi level shift. The valence band maximum (VBM) was extrapolated from linear fits of the valence band spectra obtained throughout the experiment [Fig. 1(d)]. A valence band edge shift to lower binding energy (toward the Fermi level) is an indicator of *p*-type doping induced by N_2 plasma treatment.[9] *P*-type doping behavior upon Se substitution by nitrogen is expected considering the electronegativity of nitrogen comparing to selenium.[25] After 10 min exposure to N_2 plasma, the valence band edge shifts detected from MBE WSe_2 (0.2 eV) and bulk WSe_2 (0.5 eV) were consistent with the shifts in the W 4*f* and Se 3*d* core levels. Fermi level shifts toward the valence band edge (*p*-type) were larger in bulk WSe_2 compared to MBE WSe_2 in all sets of samples investigated in this work. The difference in the Fermi level shift detected between MBE and bulk WSe_2 samples could be explained by the initial VBM position of the respective samples. The as-grown MBE film is initially *p*-type as indicated by the VBM located 0.7 eV below the Fermi level while the VBM initially detected from bulk WSe_2 is 1.2 eV below E_F. These differences could be due to extrinsic impurities in the bulk crystals.[6]

In comparison with the study on MoS_2,[16] nitrogen incorporation into WSe_2 occurs at a significantly slower rate as nitrogen is detectable after 10 min N_2 plasma exposure compared to just 2 min in the case of the same treatment applied to MoS_2. In addition, after 60 min N_2 plasma exposure, the nitrogen to tungsten ratio in WN_xSe_{2-x} is much lower than the nitrogen to molybdenum ratio in MoN_xS_{2-x} obtained after the same duration of plasma exposure.

Similar to the covalent doping of MoS_2 by N_2 plasma,[16] the incorporation of nitrogen into WSe_2 samples and formation of the W–N bond could result in compressive strain due to a smaller atomic radius of nitrogen compared to that of selenium. Raman spectroscopy is known to be a powerful tool to reveal the effect of doping on the sample structure. Raman spectroscopy was employed to qualitatively investigate the effects of N_2 plasma on lattice strain in exfoliated monolayer (ML) and bilayer (BL)

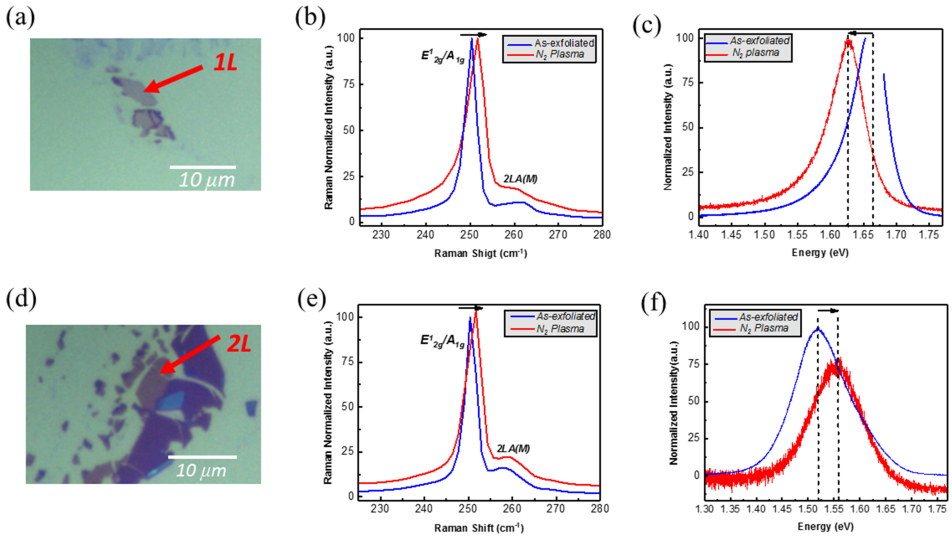

FIG. 2. Optical images of exfoliated (a) monolayer and (d) bilayer WSe_2 flakes. Raman spectra obtained from (b) monolayer and (e) bilayer WSe_2. PL spectra obtained from the same (c) monolayer and (f) bilayer WSe_2 flakes.

WSe_2 flakes. Figures 2(a) and 2(d) show optical images of ML and BL WSe_2 flakes, respectively. The separation between the peak convoluted with degenerate $E^1{}_{2g}/A_{1g}$ vibrational modes and the higher wavenumber peak corresponding with the second order Raman mode due to LA phonons at the M point in the Brillouin zone [2LA(M)][26] is a fingerprint of number of layers of WSe_2.[26,27] The separation between the degenerate $E^1{}_{2g}/A_{1g}$ peak and 2LA(M) peak detected from the flakes shown in Figs. 2(a) and 2(d) is ~11 cm^{-1} and ~6 cm^{-1}, consistent with ML and BL WSe_2, respectively [Figs. 2(b) and 2(e)]. After 10 min N_2 plasma exposure, the $E^1{}_{2g}/A_{1g}$ peak blue shifts 2.3 cm^{-1} and 1.4 cm^{-1} for the monolayer and bilayer samples, respectively. The blue shift in the $E^1{}_{2g}/A_{1g}$ peak indicates compressive strain from a reduction in the lattice constant[28] and also *p*-type doping. *P*-type doping has also been correlated with an intensity increase of the A_{1g} phonon.[9]

To examine the optical bandgap, PL spectroscopy was employed on the same exfoliated WSe_2 flakes as were probed with Raman spectroscopy. The peak position at 1.66 eV detected by PL from the ML WSe_2 flake [Fig. 2(c)] corresponds with the direct bandgap of monolayer WSe_2.[28] Monolayer WSe_2, of course, exhibits the highest PL intensity among ML, BL, Tri-layer, and quad-layer WSe_2 flakes,[26] with a maximum intensity over the limit of the detector employed in this work. Figure 2(f) shows the PL spectrum obtained from bilayer WSe_2 with peak intensity at 1.52 eV, consistent with a previous report.[28] A red shift in PL peak is detected after 10 min N_2 plasma exposure in the case of monolayer WSe_2 [Fig. 2(c)], consistent with a change in band structure due to induced strain caused by the covalently incorporated nitrogen.[28] Desai *et al.*[28] report a crossover from indirect to direct bandgap in bilayer WSe_2 is practically possible by applying strain due to the small difference between the direct and indirect bandgaps of bilayer WSe_2. As strain increases, a second peak, corresponding with the direct bandgap, appears at higher energy in the PL spectrum and increases in intensity until the indirect bandgap peak is no longer resolvable. Further increase in strain results in a red shift of the direct bandgap peak of bilayer WSe_2. In this work, the PL spectra detected from bilayer WSe_2 after 10 min N_2 plasma exposure exhibits characteristics reflecting a lesser magnitude of strain than that corresponding with a PL spectrum dominated by the direct bandgap peak as observed by Desai *et al.* Both Raman and PL provide evidence of successful nitrogen incorporation at the surface of mono and bilayer WSe_2 flakes resulting in *p*-type doping and inducing strain.

This work demonstrates covalent *p*-type doping of both MBE and bulk WSe_2 via a remote N_2 plasma treatment. However, surface roughening and/or etching could be an undesirable side effect of the N_2 plasma exposure to WSe_2 in a device fabrication procedure.[23] The WSe_2 surface topography after N_2 plasma exposure was evaluated by AFM and STM. Figure 3(a) shows the flat

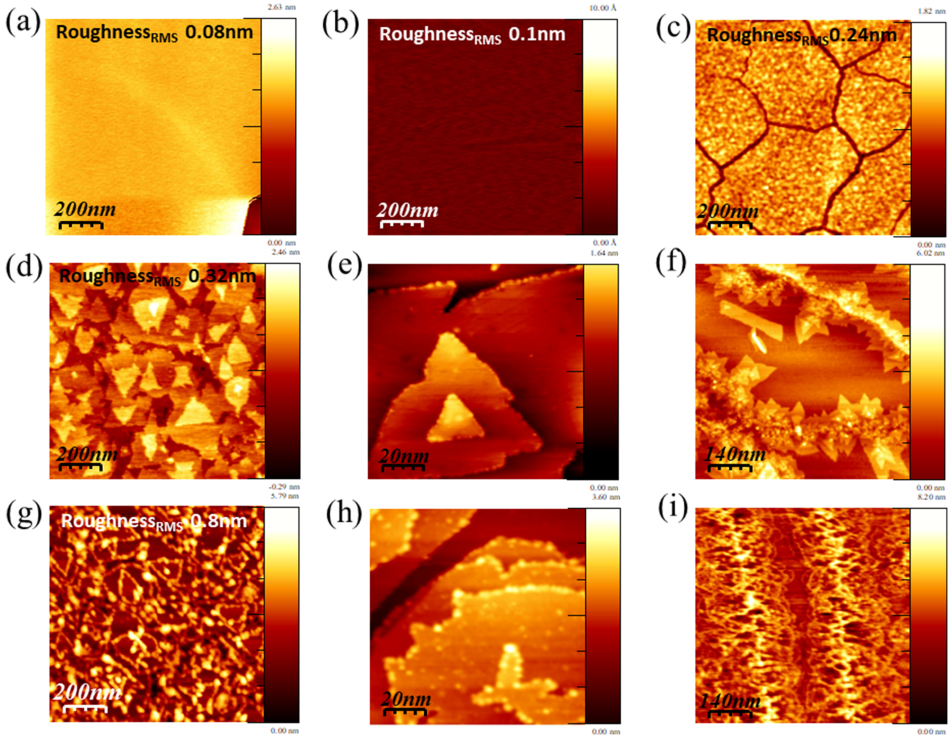

FIG. 3. AFM images obtained from exfoliated WSe_2 (a) before treatment, (b) after 15 min, and (c) after 60 min N_2 plasma exposure. AFM images of MBE WSe_2 (d) before treatment and (g) after 15 min N_2 plasma exposure. STM images obtained from the same MBE WSe_2 [(e) and (f)] before N_2 plasma treatment with the tip bias of 1.8 V and tunneling current of 300 pA and [(h) and (i)] after 30 min treatment with tip bias of 2 V, 1.8 V, and tunneling current of 200 pA.

surface of bulk WSe_2 before N_2 plasma treatment. After N_2 plasma exposure for 15 min, there are no obvious topographical changes [Fig. 3(b)] in the surface of bulk WSe_2 consistent with an analogous N_2 plasma treatment on bulk MoS_2 for short exposure times (15 min).[16] After 60 min of the N_2 plasma treatment, significant changes in the surface structure appear in the form of cracks with depth of ~0.7 nm, the height of one layer of WSe_2 [Fig. 3(c)]. Well-defined, mono and few-layer triangular WSe_2 domains with sharp (oxidation-free) edges are observed on the as-grown MBE WSe_2 surface [Fig. 3(d)]. After 15 min N_2 plasma exposure, the AFM image in Fig. 3(g) indicates a strong edge decoration on all WSe_2 domains suggesting that nitrogen preferentially reacts with the edges.

The contrast at the as-grown WSe_2 domain edges is comparable with that of the terraces suggesting the surface potential is similar across the probed region. However, N_2 plasma exposure for 30 min results in a sharp contrast between the terraces (dark) and domain edges (bright, difference in the electron density, and/or the height), which corresponds to significant change in surface potential in the vicinity of the domain edges [Figs. 3(e) and 3(h)]. Edge roughening observed in AFM images concomitant with the edge localized contrast variation detected with STM suggests that nitrogen preferentially nucleates at WSe_2 edges, which are known to be more reactive than the WSe_2 basal plane.[29] The contrast variation observed in STM images could relate to the metallic character of the W–N bond, and the tunneling current is higher in these areas compared with the adjacent semiconducting WSe_2. Figures 3(f) and 3(i) present STM images obtained from the MBE WSe_2 film, showing a high density of WSe_2 domains at HOPG step edges with small domain size as previously reported.[17] Following 30 min remote N_2 plasma treatment, there is a noticeable degradation of the surface as evidenced by a large increase in surface roughness [Fig. S4(b) of the supplementary material]. Damage is observed across the entire surface of smaller MBE WSe_2 domains (Fig. S4 of the supplementary material). In contrast, large MBE WSe_2 domains appear to only be affected on the edges [Fig. 3(h)]. Both AFM and STM results suggest that nitridation occurs preferentially at

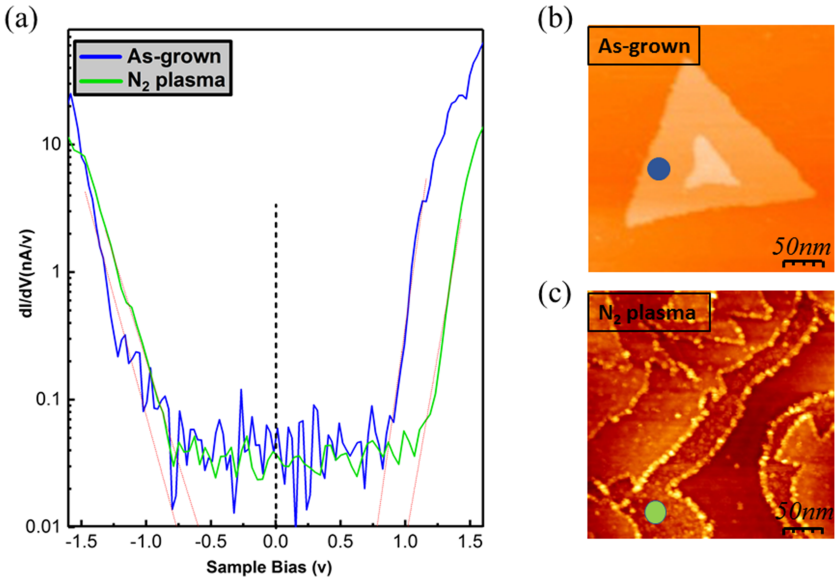

FIG. 4. (a) Comparison of scanning tunneling spectroscopy spectra measured (b) before N_2 plasma treatment with tip bias of 2 V and tunneling current of 300 pA (blue) and (c) after 30 min N_2 plasma treatment with the tip bias of 1.5 V and tunneling current of 500 pA (red). The valence band maximum (VBM) and conduction band minimum (CBM) was measured on as-grown MBE WSe_2 monolayer at −0.98 eV and 0.85 eV, respectively. Following 30 min N_2 plasma treatment, the VBM (CBM) was measured at 1.14 eV (−0.67 eV).

the domain edges prior to affecting the WSe_2 terraces. Figure 4 displays the STS spectra obtained from an MBE WSe_2 monolayer prior to and following N_2 plasma treatment. A 1.83 eV bandgap is measured from as-grown monolayer WSe_2 with no significant changes induced by the N_2 plasma treatment (1.81 eV after 30 min exposure). The Fermi level moves toward the valence band maximum (VBM) by 0.3 eV in agreement with the Fermi level shift observed by XPS. This is further evidence that N_2 plasma exposure induces *p*-type doping in MBE WSe_2.

In summary, the effects of N_2 plasma exposure on the electronic and structural properties of MBE thin films and bulk WSe_2 are evaluated using XPS, Raman, PL, AFM, and STM. The appearance of an additional chemical state in the W 4*f* core level in conjunction with increased nitrogen concentration above the limit of XPS detection following N_2 plasma exposure indicates that nitrogen forms a covalent bond with tungsten. Shifts detected in characteristic WSe_2 vibrational modes and the PL peak after N_2 plasma exposure suggest that incorporating nitrogen into the WSe_2 lattice in the form of covalent W–N bonds induces strain in both MBE and bulk WSe_2. In addition, AFM and STM images indicate that N_2 plasma exposure damages the WSe_2 surface after longer exposure times eventually resulting in the formation of cracks in the case of bulk WSe_2, while the remote N_2 plasma process employed here is more destructive to few-layer MBE WSe_2 compared to bulk WSe_2. Tuning the duration of N_2 plasma exposure offers control over the amount of strain induced in the WSe_2 structure, both bulk and MBE, and can pave the ground for engineering the bandgap and electronic properties of WSe_2.[30]

See supplementary material for the O 1*s* and C 1*s* core levels and Valence Band Maximum of MBE and exfoliated WSe_2 prior to load them into UHV system and after annealing, the sequential N_2 plasma exposure and gradual intensity increase of W–N peak is demonstrated, the angle resolved XPS in bulk sensitive angle from both samples is provided, XPS spectra from HOPG as a substrate after N_2 plasma exposure, and STM image from MBE WSe_2 after 30 min N_2 exposure is included.

This work is supported in part by the Center for Low Energy Systems Technology (LEAST), one of six centers supported by the STARnet phase of the Focus Center Research Program (FCRP), a Semiconductor Research Corporation program sponsored by MARCO and DARPA. Also, by the Southwest Academy on Nanoelectronics (SWAN) sponsored by the Nano-electronic Research

Initiative and NIST and in part by NSF Award No. 1407765 under the US/Ireland UNITE collaboration. The authors acknowledge Dr. Lanxia Cheng for useful discussions on the Raman and PL study.

[1] W. Liu, J. Kang, D. Sarkar, Y. Khatami, D. Jena, and K. Banerjee, Nano Lett. **13**(5), 1983–1990 (2013).
[2] H. Fang, S. Chuang, T. C. Chang, K. Takei, T. Takahashi, and A. Javey, Nano Lett. **12**(7), 3788–3792 (2012).
[3] B. W. Baugher, H. O. Churchill, Y. Yang, and P. Jarillo-Herrero, Nat. Nanotechnol. **9**(4), 262–267 (2014).
[4] A. Pospischil, M. M. Furchi, and T. Mueller, Nat. Nanotechnol. **9**(4), 257–261 (2014).
[5] M. Deshpande, G. Solanki, and M. Agarwal, Mater. Lett. **43**(1), 66–72 (2000).
[6] R. Addou and R. M. Wallace, ACS Appl. Mater. Interfaces **8**(39), 26400–26406 (2016).
[7] V. Podzorov, M. Gershenson, C. Kloc, R. Zeis, and E. Bucher, Appl. Phys. Lett. **84**(17), 3301–3303 (2004).
[8] M. Tosun, L. Chan, M. Amani, T. Roy, G. H. Ahn, P. Taheri, C. Carraro, J. W. Ager, R. Maboudian, and A. Javey, ACS Nano **10**(7), 6853–6860 (2016).
[9] D.-H. Kang, J. Shim, S. K. Jang, J. Jeon, M. H. Jeon, G. Y. Yeom, W.-S. Jung, Y. H. Jang, S. Lee, and J.-H. Park, ACS Nano **9**(2), 1099–1107 (2015).
[10] K. Chen, D. Kiriya, M. Hettick, M. Tosun, T.-J. Ha, S. R. Madhvapathy, S. Desai, A. Sachid, and A. Javey, APL Mater. **2**(9), 092504 (2014).
[11] H. Fang, M. Tosun, G. Seol, T. C. Chang, K. Takei, J. Guo, and A. Javey, Nano Lett. **13**(5), 1991–1995 (2013).
[12] C.-H. Chen, C.-L. Wu, J. Pu, M.-H. Chiu, P. Kumar, T. Takenobu, and L.-J. Li, 2D Mater. **1**(3), 034001 (2014).
[13] P. Zhao, D. Kiriya, A. Azcatl, C. Zhang, M. Tosun, Y.-S. Liu, M. Hettick, J. S. Kang, S. McDonnell, and K. C. Santhosh, ACS Nano **8**(10), 10808–10814 (2014).
[14] K. Akada, T.-O. Terasawa, G. Imamura, S. Obata, and K. Saiki, Appl. Phys. Lett. **104**(13), 131602 (2014).
[15] A. Talbi, Z. Benamara, B. Akkal, B. Gruzza, L. Bideux, C. Robert, C. Varenne, and N. Chami, Mater. Sci. Eng.: A **437**(2), 254–258 (2006).
[16] A. Azcatl, X. Qin, A. Prakash, C. Zhang, L. Cheng, Q. Wang, N. Lu, M. J. Kim, J. Kim, and K. Cho, Nano Lett. **16**(9), 5437–5443 (2016).
[17] R. Yue, Y. Nie, L. Walsh, R. Addou, C. Liang, N. Lu, A. Barton, H. Zhu, Z. Che, and D. Barrera, 2D Mater. **4**, 045019 (2017).
[18] R. M. Wallace, ECS Trans. **16**(5), 255–271 (2008).
[19] A. Herrera-Gomez, A. Hegedus, and P. Meissner, Appl. Phys. Lett. **81**(6), 1014–1016 (2002).
[20] R. Addou, L. Colombo, and R. M. Wallace, ACS Appl. Mater. Interfaces **7**(22), 11921–11929 (2015).
[21] I. Horcas, R. Fernández, J. Gomez-Rodriguez, J. Colchero, J. Gómez-Herrero, and A. Baro, Rev. Sci. Instrum. **78**(1), 013705 (2007).
[22] K. Schmid, A. Manhard, C. Linsmeier, A. Wiltner, T. Schwarz-Selinger, W. Jacob, and S. Mändl, Nucl. Fusion **50**(2), 025006 (2010).
[23] D. Alegre, T. Acsente, A. Martin-Rojo, E. Oyarzabal, F. Tabares, G. Dinescu, G. De Temmerman, R. Birjega, C. Logofatu, and J. Kovac, Rom. Rep. Phys. **67**(2), 532–546 (2015).
[24] M. Nagai, T. Suda, K. Oshikawa, N. Hirano, and S. Omi, Catal. Today **50**(1), 29–37 (1999).
[25] Y. Zhang, Inorg. Chem. **21**(11), 3886–3889 (1982).
[26] W. Zhao, Z. Ghorannevis, K. K. Amara, J. R. Pang, M. Toh, X. Zhang, C. Kloc, P. H. Tan, and G. Eda, Nanoscale **5**(20), 9677–9683 (2013).
[27] H. Sahin, S. Tongay, S. Horzum, W. Fan, J. Zhou, J. Li, J. Wu, and F. Peeters, Phys. Rev. B **87**(16), 165409 (2013).
[28] S. B. Desai, G. Seol, J. S. Kang, H. Fang, C. Battaglia, R. Kapadia, J. W. Ager, J. Guo, and A. Javey, Nano Lett. **14**(8), 4592–4597 (2014).
[29] R. C. Longo, R. Addou, K. Santosh, J.-Y. Noh, C. M. Smyth, D. Barrera, C. Zhang, J. W. Hsu, R. M. Wallace, and K. Cho, 2D Mater. **4**(2), 025050 (2017).
[30] P. Johari and V. B. Shenoy, ACS Nano **5**(7), 5903–5908 (2011).